

PASSIVE FLOW CONTROL DEVICES ON LOW-REYNOLDS DU89-134 AIRFOIL

Carlo Brunelli^{1,2,3}, Matija Avirović^{1,3,4}, Bart Janssens¹, Benoît G. Marinus¹, Mark Runacres², Georg May³, Antoine Ecorce⁵ & Antonin Dalbera⁵

¹Royal Military Academy, Renaissancelaan 30, Brussels, 1000, Belgium

²Vrije Universiteit Brussel, Brussels, 1050, Belgium

³Von Karman Institute for Fluid Dynamics, Sint-Genesius-Rode, 1640, Belgium

⁴Ghent University, Ghent, 9000, Belgium

⁵National Polytechnic Institute of Toulouse - École nationale supérieure d'électrotechnique, d'électronique, d'informatique, d'hydraulique et des télécommunications (ENSEEIHT), Toulouse, France

Abstract

Passive Flow Control abstract

Keywords: low-Reynolds, passive flow control, laminar separation bubble, transition

1. Introduction

1.1 Context

The constant search for improved aerodynamic performance in the cruise phase of an aircraft is a never ending challenge for researchers and engineers. The focus is basically to save fuel, improve endurance, and be more appealing to industry and stakeholders. In recent years, High-Altitude Pseudo Satellites (HAPS) have appeared and are beginning to be operational. They represent a remarkable and innovative category of aircraft that is designed to operate at stratospheric altitudes (12-20 km), [1]. They provide a cost-effective and sustainable alternative to conventional satellite-based systems and have the potential to revolutionize long-duration missions. As HAPS capabilities continue to evolve, optimizing their performance, especially in the cruise phase, becomes a central imperative. As proved in [2], Passive Flow Controls (PFCs), in specific vortex generators, can have a positive effect in increasing the maximum lift-to-drag ratio and postponing the stall angle for low-Reynolds number airfoils. Güler et al. [3] investigated numerically the effect of installing riblets over a NACA0018 airfoil at different locations for Reynolds number 100000. It shows that the use of transverse riblets remarkably affects flow characteristics, delaying the angle of stall.

1.2 Low-Reynolds

This article will focus on flows with low-Reynolds numbers, where boundary layer transition and separation become significant factors [4]. In aeronautics, a low-Reynolds usually means a Reynolds in the range 10^4-10^6 [1]. Under such flow conditions, laminar flow predominates. Consequently, at this Reynolds number, the boundary layer tends to be unstable and can separate and/or become turbulent. Separation can result in the formation of a recirculating flow, the phenomenon known as the Laminar Separation Bubble (LSB), figure 1 provided the separated layer reattaches after having undergone transition to turbulent. The formation of an LSB substantially impacts aerodynamic coefficients, lift, and drag [5].

Numerical and experimental studies on the DU89-134 airfoil show the presence of an LSB on the suction side at Reynolds $500\,000$ and angle of attack 5° , [6]. It has also been shown how the laminar-to-turbulent transition plays a fundamental role in the position of the bubble itself. This is the parameter that PFCs will most influence, as reported by Güler et al. [3].

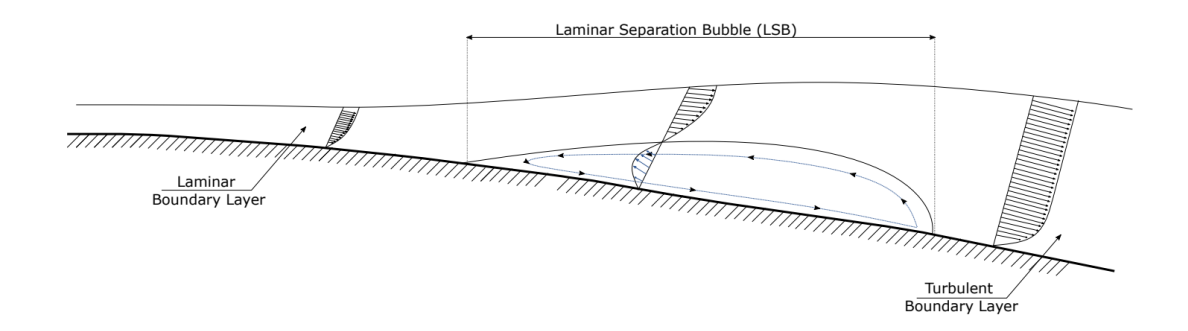


Figure 1 – Laminar Separation Bubble scheme

2. Objective

This paper aims to better understand how different PFCs interact with the LSB and how they can impact locally the flow field and the overall aerodynamic performance. In this study, different CFD software packages were used: STARCCM+ [7], Ansys Fluent [8] and XFOIL [9], to have a comparison between different solvers. Furthermore, this study is also based on wind tunnel modeling, where numerical simulations are carried out to be as close to reality as possible. The following PFCs are going to be simulated and tested:

- · Clean profile no PFC
- · Triangular trip strips
- · Slotted airfoil straight

The configurations are analyzed mostly numerically using 3D steady RANS. The numerical results are compared with experimental results obtained thanks to infrared thermography, oil flow visualization, and pressure taps. More details on the wind tunnel and experimental techniques can be found in [6].

3. Passive Flow Control Tecniques

Various passive flow control techniques have been used and tested over the years to control the formation of LSB. Genç et al. [10] provides a comprehensive review of the most common and their effects on LSB. One of the main advantages of passive flow control techniques is that they are relatively simple and inexpensive to implement compared to other types of active flow control mechanisms. They do not require additional power or control systems and can be easily integrated into the design of a standard airfoil. However, they have some limitations, they cannot switch on/off, are designed for cruise conditions, and this can reduce performances in take-off and landing phases. Passive flow devices can increase the airfoil design's complexity, making it more difficult to manufacture and maintain. They can also increase the level of airfoil acoustic noise, [11], thereby increasing self-noise due to turbulence interaction with the trailing edge.

3.1 Vortex Generators

Vortex generators (VGs) are the most straightforward and fairly effective flow control devices to avoid flow separation. A vortex generator is usually a small device placed on a wall to induce a vortex in the streamwise direction. They can have many shapes: triangular, quadrangular, wedge, etc. When vortex generators are adopted for flow control, they are usually aligned in one row along the spanwise direction, as reported by Wang and Feng [11], picture 2. An extensive experimental campaign has been carried out by Seshagiri et al. [2] on low-Reynolds airfoils to study the effects of VGs. The results suggest that the static VGs work in a similar manner as those at higher Reynolds numbers allowing and increasing the maximum lift coefficient and stall angle. At low AoA, the VGs may reduce drag by limiting the length of the bubble, thereby reducing pressure drag.

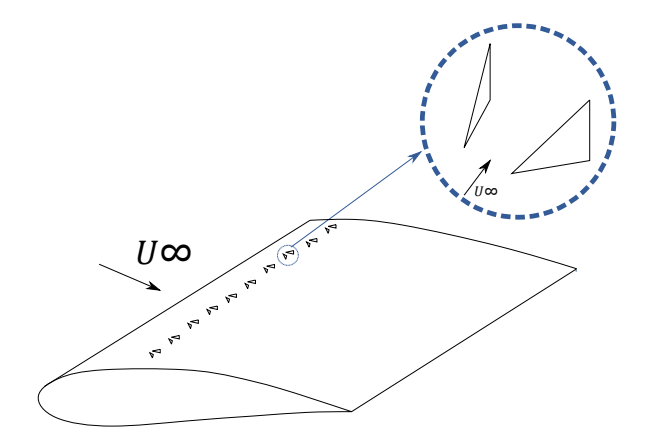


Figure 2 – Vortex Generators, adapted from [10]



Figure 3 - Slotted E387 airfoil

The height of vortex generators is usually between $1.2 - 0.4\delta$. There are also the *micro vortex-generators* whose height is on the order of magnitude 0.1δ .

3.2 Dimples or trip strips

The dimples, trip strips, or transverse riblets represent the most simple family of passive flow control. They are controlled imperfections in the airfoil that represent an obstacle to the flow and trigger separation or turbulent transition. They can have various shapes, such as triangles, spheres, or cubes. In [3], the effect of trip strips at different positions on a NACA 0018 airfoil for Reynolds number $100\,000$ is investigated numerically. The study shows an increase in lift for 8° and 10° and a delay in the stall angle from 13° to 15° . Sefiddashti et al. [12] have experimentally tested circular cross-section trip strips - oriented in the streamwise direction - in the transient flow regime: Reynolds number 2.02×10^5 , 1.4×10^5 . The research points out that the extent of the effect of the riblets on the aerodynamic performance of the airfoil depends on the angle of attack, Reynolds number, and strips positioning. The maximum drag reduction is measured at 6° of angle of attack.

3.3 Slotted airfoil

The slotted airfoil consists in creating a gap near the leading edge. It allows the high-pressure air from beneath the wing to flow over the suction side surface of the wing. This creates a small vortex that increases the velocity of the flow at the exit of the slot. This vortex helps delay the separation. The slot technique changes the aerodynamic characteristics of the air passing over the wing, and not the shape of the wing itself. Kumar et al. [13] perform a numerical analysis on the E387 airfoil at Reynolds number $100\,000$ to investigate the effects of slot configuration. They noted that orientation, thickness and positions of the slot are the main parameters influencing the aerodynamic performances, obtaining a drag reduction for a slot oriented at 30° and a convergent exit.

4. Method and setup

4.1 Physical conditions

The design point for testing the devices is Reynolds number $500\,000$ - respecting the low-Reynolds definition, and angle of attack 5° . In standard operational conditions, the airfoil operates within 1° and 5° angle of attack. The highest angle has been chosen because in experiments as well as in numerical simulations in [3], [10], [2], [12] the angle of attack is minimum 8° . In general, they delay the flow separation inducing the transition.

Turbulence Intensity (TI) is a physical quantity that plays a key role in this regime, [5], [14], [15]. It is defined as $TI = \frac{u'}{U_{\infty}}$, where u' is the root-mean-square of U_{∞} . In the simulations, a TI = 0.20%

is reached in the wind tunnel test section, [6]. This value is based on experimental measurements obtained with the hot wire method.

4.2 Domain and boundary conditions

Wind tunnel testing was carried out at the Royal Military Academy by Avirović et al. [6] in the $0.6\,\mathrm{m} \times 0.6\,\mathrm{m} \times 1.2\,\mathrm{m}$ open-circuit low-speed wind tunnel. The airfoil model has a chord of $0.20\,\mathrm{m}$. Althaf at al. [16] performed numerical modeling of low-speed wind tunnels. They concluded that inlet velocity profiles do not have a significant impact on the flow in the test section; the converging duct seems to attenuate any differences in the inlet profiles. For this reason, a uniform inlet velocity is used. Furthermore, they also claim that the compressibility effects under Mach number 0.2 are negligible - which is the case. Additionally, only a slice - with constant depth - of the wind tunnel has been considered. The wall conditions on the upper and lower walls and symmetry conditions on the side walls of the slice are implemented, figure 4.

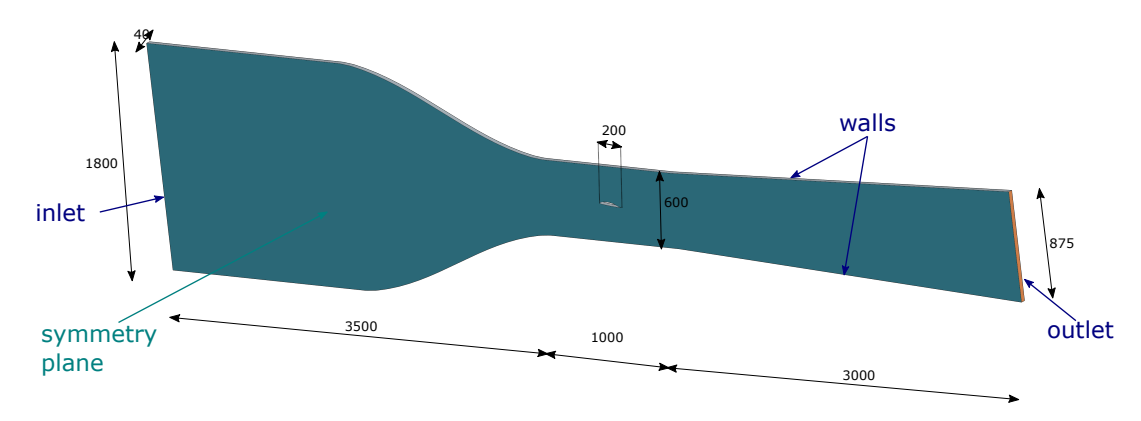


Figure 4 – Wind tunnel *slice* and dimensions in mm

This method allows for the influence of the convergent duct while leaving the direction of the streamlines near the airfoil free. This representation does not precisely take into account the influence of the four walls, but only the influence of two of them. In addition, this model reduces the 3D effects, specifically in the convergent duct.

4.3 RANS Numerical model

3D-RANS simulations of the flow around the airfoil are performed with the transitional $\gamma - Re_{\theta}$ SST turbulence model integrated within the commercial software ANSYS Fluent (version 2022R1) and Simcenter STAR-CCM+ (version 2302). The transitional SST model couples the shear-stress transport model $k - \omega$ SST developed by Menter with the transport equations for the intermittency and transition momentum thickness Reynolds number $\gamma - Re_{\theta}$. It has been proven to properly model the laminar-turbulent transition at low Reynolds, [5] and [4]. All the simulations are solved as steady.

4.4 XFOIL calculations

3D-RANS simulations are complemented with XFOIL calculations, [17], to employ an additional source of data that would eventually enable us to ensure the viability of our results. XFOIL uses a panel method to calculate the pressure and shear stress distribution around an airfoil, taking into account crucial factors such as angle of attack and the Reynolds number, [18]. Furthermore, this tool enables the prediction of boundary layer behavior and facilitates the analysis of how modifications to the airfoil's shape impact its performance. The amplification factor is set as $N_{crit} = 10$. The value of N_{crit} is a measure of free-flow turbulence and is used to simulate the transition location, [19].

4.5 Experimental setup

The experimental measurements have been performed at the Royal Military Academy low-speed and low-turbulence wind tunnel depicted in detail in [6]. The DU89-134 wind tunnel airfoil model was constructed from three separate 3D-printed segments. Each segment was printed using Formlabs Grey Resin V4 with a Formlabs Form 3 stereolithography 3D printer, set to a layer height of 0.05

mm. The joints between the segments were seamlessly integrated with body filler, which was sanded smooth after hardening. The assembled DU89-134 airfoil had a chord length of $c=0.2\,\mathrm{m}$ and a span of $s=0.595\,\mathrm{m}$, with an average surface roughness of $R_a=2.71\,\mu\mathrm{m}$. The modular design allowed quick change between different PFC configurations by swapping the middle section of the test airfoil. The Infrared Thermography (IRT) measurement setup is depicted in Fig. 5 and consists of a FLIR A655sc long wave IR camera, germanium glass window and HOENLE Superspot 575 halogen heating array. The IR camera has a resolution of 640×480 pixels and Noise Equivalent Temperature Difference (NETD) lower than $30\,\mathrm{mK}$.

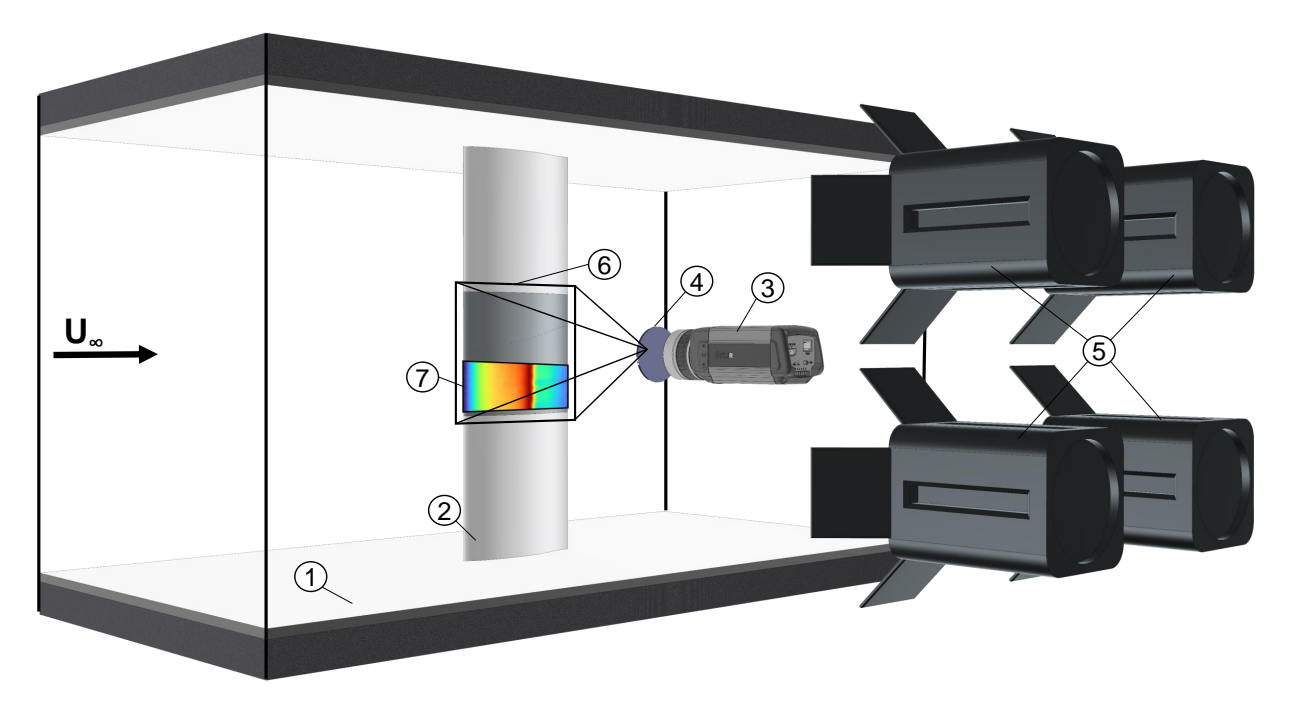


Figure 5 – 1-Wind tunnel test section, 2-DU89-134 airfoil, 3-Infrared camera, 4-Germanium window, 5-Halogen lamps, 6-IR camera FOV, 7-IR region of interest

The measurement protocol involves heating the airfoil using a halogen heating array while the wind tunnel is turned off. Once a uniform airfoil surface temperature is reached the wind tunnel is turned on and after quasi-steady conditions are met the IR images are acquired. Mean streamwise locations of Laminar separation, transition and reattachment have been determined according to the procedure described in [20], where the maximal value of the surface temperature gradient corresponds to laminar separation, minimal value to the transition location and minimal local temperature to reattachment respectively.

5. PFCs Modellization

5.1 Trip strips

The effects of the trip strips on the airfoil performance are studied on STARCCM+. The idea is to add a transverse riblet, an obstacle, perpendicular to the flow direction, and to evaluate the effect on the lift and drag ratio. The geometry of the airfoil is changed only in a specific location. It is important to note that the mesh is locally refined, where the strip is located, to capture the rapid change in the properties of the flow. Different locations of the strips have been tested: from 30% up to 80% of the chord. However, a trip strip in the last 20% of the chord would have a minimum impact, the flow is most likely already separated and turbulent, this assumption has been verified from the clean profile simulation. The size of the trip strip has been chosen following the same dimensions reported in [3] and [12], with a height of $1 \, \text{mm}$ (0.5% of the chord).

5.2 Slotted airfoil

The slotted airfoil effect was also re-created in STARCCM+. The idea is to cut the airfoil in two sections, creating a duct between suction and pressure side. In such way, some air will flow from the

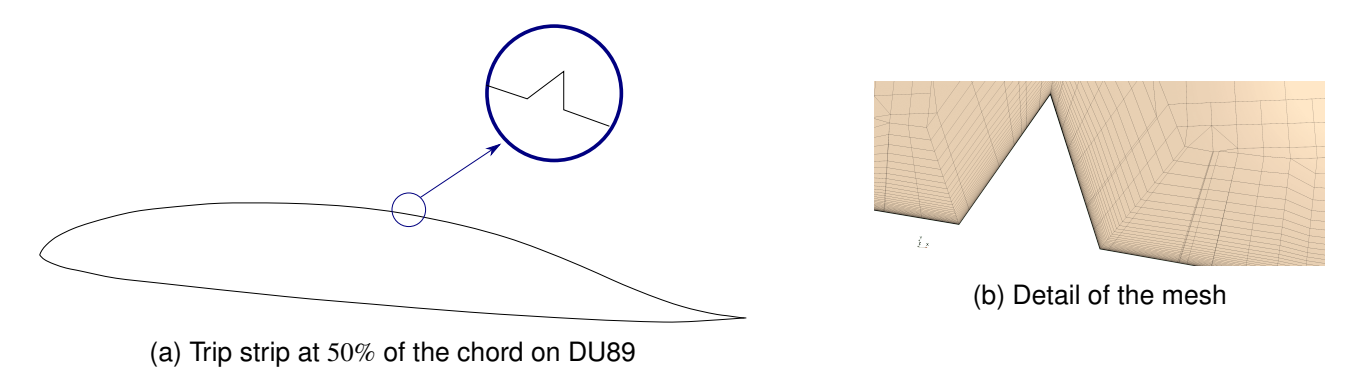


Figure 6 – Triangular trip strip

lower (high-pressure side) towards the top (low-pressure side), thereby re-energizing the flow thence postponing the boundary layer separation. Several geometrical parameters have to be considered to create the configuration. For choosing dimensions and position of the cut, the reference study is [13] where cuts with a variable inclination of 12.97° , 30° , 60° , 90° have been simulated. In figure 7b Ψ represents the angle of the inclination of the cut w.r.t chord line, ζ the position on the suction side of the slot and L is the width of the cut. Two different opening size have been tested: $L=0.002\,\mathrm{m}$ and $L=0.004\,\mathrm{m}$ (denoted as Large). The cuts are always a constant width, it is neither diverging or converging. In this new configuration, it is important to note that it is necessary to adapt the mesh according to the settings used previously to preserve a prism layer to capture air flowing inside the airfoil, [21]. In table 1 the parameters and their range are reported.

Parameter	Values	Parameter description
Ψ[°]	[15;30]	Angle which governs the inclination of the cut
ζ [x/c]	[0.45; 0.5; 0.6]	Top cut placement
L [x/c]	[0.01;0.02]	Length which governs the width of the cut

Table 1 – List of the parameters used in the different configurations of the slotted airfoil where $c=0.20\,\mathrm{m}$

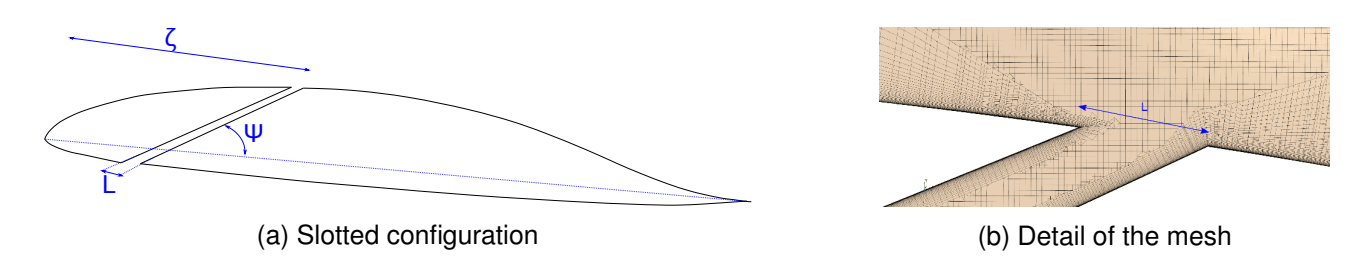


Figure 7 – Slotted configuration

6. Results

The clean configuration refers to the airfoil without any added device and a smooth surface.non-intrusive for the clean airfoil have been carried out with Ansys Fluent, STARCCM+ and XFOIL and compared with experimental results to verify the CFD set-up.

6.1 Clean profile

The results obtained with the different software are reported in table 2 and they are compared with the experimental values found in [6].

 C_p and C_f curves, figure 8, are almost overlapping for Ansys Fluent and STARCCM+, they numerically predict the development of an LSB on the suction side and only minor discrepancies arise in the last 10% of the chord. The location of the separation point on the suction side computed numerically also matched the experimental evidence. However, both solvers anticipate by 5% of the chord

	Experiment [6]	STARCCM+	Ansys Fuent	XFoil
$\overline{C_L}$	0.77	0.79	0.79	0.99
C_D	0.017	0.018	0.013	0.0091
Separation point (x/c)	0.62	0.55	0.55	0.59
Reattachment point (x/c)	0.74	0.69	0.69	-

Table 2 – DU89-134 at Re 500000, AoA 5°, clean configuration

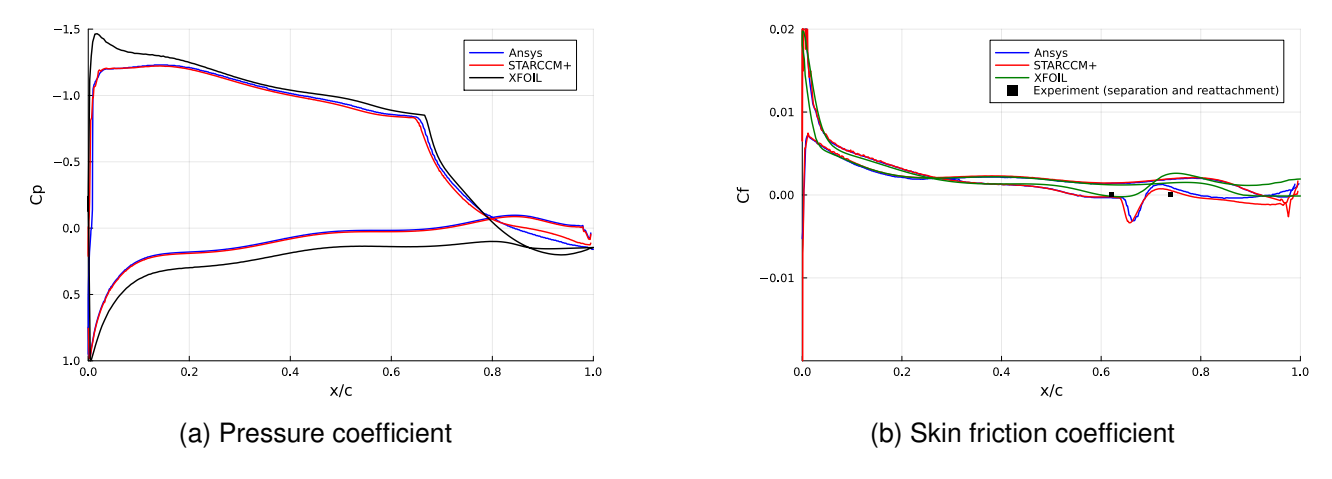


Figure 8 – C_p , C_f DU89-134 at Re 500000, AoA 5° , clean configuration

the reattachment point. It translates into aligned values for aerodynamic performance C_L and C_D between STARCCM+, Ansys Fluent and experiments. By contrast, XFOIL, seems to fail to capture the formation of an LSB consequently the whole flowfield is affected.

6.2 Trip strips

Simulations have been performed placing a single trip strip in 6 different locations on the suction side of the airfoil: x/c = [0.3, 0.4, 0.5, 0.6, 0.7, 0.8]. Figures 9a 9b report a comparison of C_p and C_f curves between the clean airfoil and two configurations with a riblet at 0.3c and 0.7c. The plots clearly show a difference in positioning the PFC device before (0.3c) or after (0.7c) the LSB develops on the clean airfoil.

The trip strip at 0.3c increases the flow pressure in front, reducing the lift contribution. Before the strip, the flow separates but remains laminar, figure 11a. After the obstacle, the flow separates, transitions to turbulent, and reattaches on the airfoil at 0.38c. It creates a bubble immediately after the trip strip and it is not an LSB because the flow is not in a laminar state. The flow reattaches and, differently from the clean configuration, the flow is now turbulent. In figure 9b, in the central part of the suction side, the friction coefficient of the trip strip configuration 0.3c is higher than the one from a clean configuration where the flow is laminar. This is leading to higher C_f which inevitably leads to a higher drag, as reported in table In this configuration, the flow separates again from the airfoil around 0.75c. The LSB phenomena does not occur anymore for this configuration.

The trip strip placed at 0.7c has a milder effect compared to one at 0.3c since it is located after separation and reattachment. The pressure of the flow approaching the strip is higher than the clean airfoil but lower than that of the trip at 0.3c as expected. Unlike the latter case, the LSB is still developing, but in a different location. The flow is energized by the turbulence created by the strip, mixing the slower boundary layer with the high momentum fluid in the outer part anticipating separation and transition of the flow, as reported in figure 9b. It has a similar effect as increasing the intensity of free-flow turbulence, [22, 14]. From the CFD simulation, the turbulence introduced by the strip in this configuration is not enough to prevent the development of the LSB. After the LSB the flow is no longer reattaching. The end of the LSB approaches the location of the strip which behaves as an obstacle for reattachment.

The differences between separated and attached flow for different strips locations are synthesized in figure 11.

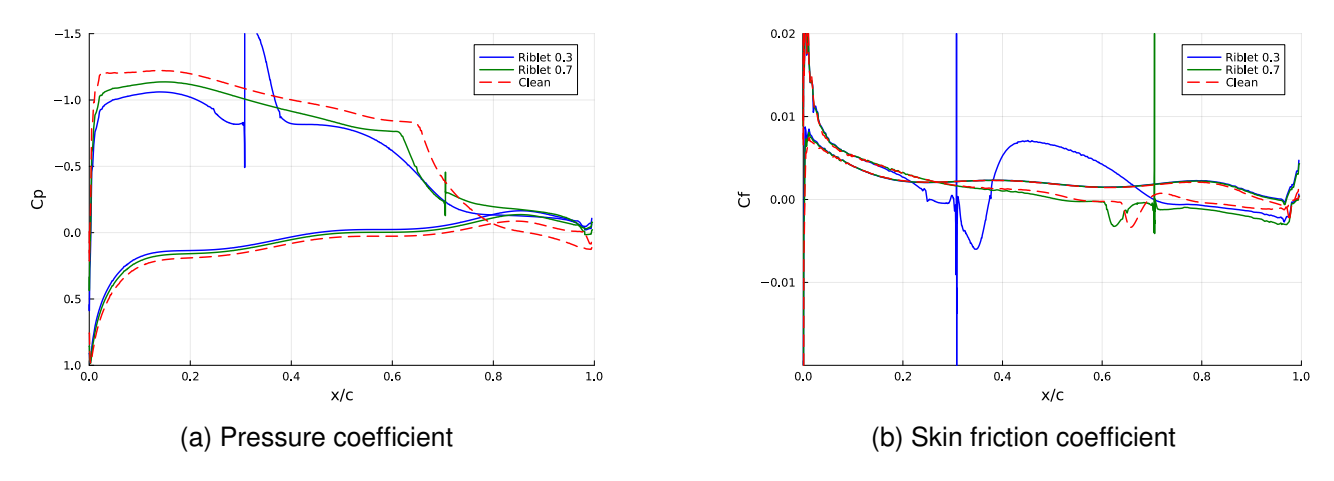


Figure 9 – C_p , C_f DU89-134 at Re 500000, AoA 5° comparison between clean airfoil, trip strip at 30% and 70% at the chord

strip position	clean airfoil	0.3 c	0.4c	0.5 c	0.6c	0.7 c	0.8 c
C_L	0.8241	0.6772	0.719	0.73	0.739	0.7448	0.8145
C_D	0.01454	0.025	0.023	0.0223	0.023	0.0221	0.015
C_L/C_D	56.7	27.1	31.9	32.8	32.3	33.7	52.9

Table 3 – Comparison of the aerodynamic performance of different strip trip positions

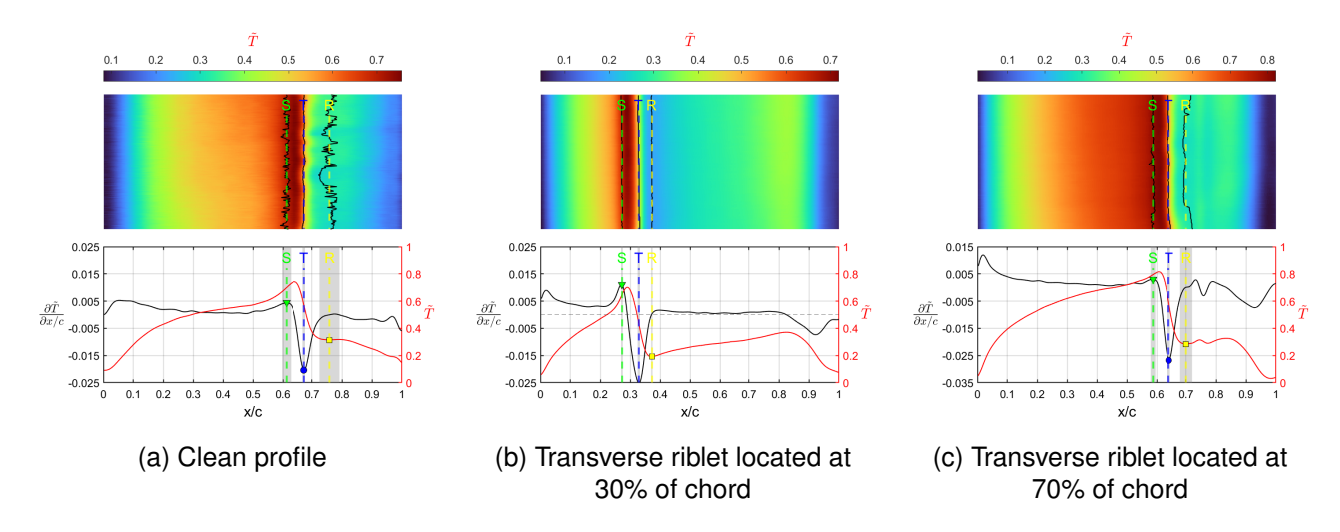


Figure 10 – Comparison between the IR images, non-dimensionalized surface temperature distributions and surface temperature gradients for the DU89-134 airfoil at Re $500\,000$ and AoA 5°

As evidenced thus far, the location of the device on the airfoil surface significantly influences its impact on the flow dynamics. Depending on its position, the device can either preserve or prevent the formation of the LSB. The strip induces an increase in pressure along the rear portion of the suction side, which plays a crucial role in generating lift. However, this pressure increase ultimately proves detrimental to aerodynamic efficiency in the tested configurations. The locations of separation, reattachment, and transition for the different cases have been validated using the non-intrusive experimental IRT technique. While this technique does not directly measure the friction coefficient, it effectively identifies the aforementioned points. The IRT results indicate that separation and reattachment occur at the same locations predicted by the RANS simulations, thereby validating the numerical setup employed.

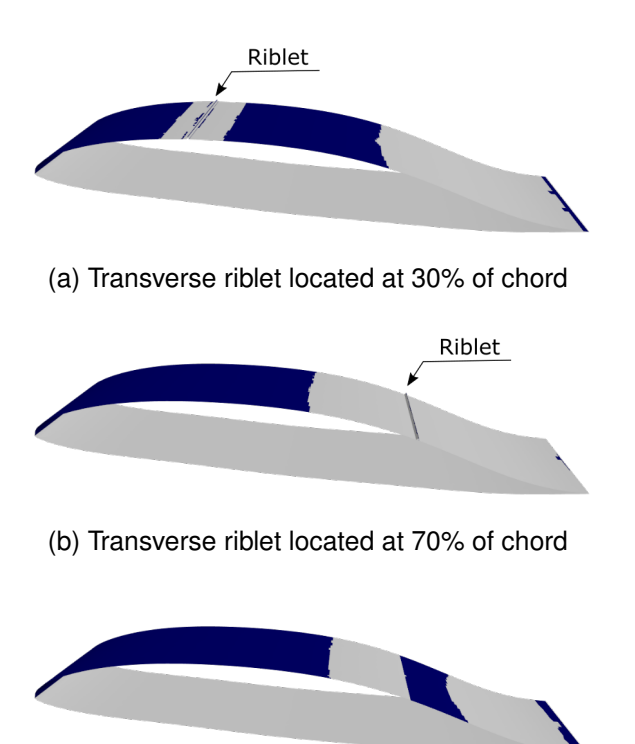


Figure 11 – Views showing the attached (blue) and separated (gray) flow regions at AoA 5° and Re 500 000 and the transverse riblet location

(c) Clean profile

6.3 Slotted airfoil

Simulations have been done for 12 different configurations in which the top position of the cut (ζ) , the inclination (Ψ) , and the width (L) vary. In tables 4 and 5 is observed that the airfoil's lift and drag coefficients are significantly impacted by all the aforementioned factors. The numerical findings indicate that adding a slot within the selected orientations to the DU89-134 airfoil results in a reduction of aerodynamic efficiency on this airfoil for the chosen configuration. Similar results have also been obtained in [13] by means of CFD analysis at Reynolds 10^5 , low inlet freestream turbulence TI = 0.11% on the E387 airfoil.

Figure 12 shows for a specific case, $\zeta=0.5$, $\Psi=15^\circ$, how the width of the slot influences the pressure and friction distribution over the airfoil. The main differences with a clean airfoil are on the suction where the air coming from the bottom is injected. Trivially, the air moves from high-pressure to low-pressure areas. That also undermines the build up of a pressure difference between the pressure and suction sides. The drastic difference from the clean geometry in C_p on the suction side justifies the reduction in C_L using this PFC configuration. In the case of the small slot, the jet moves the turbulent transition from approximately $0.68\,\mathrm{c}$ to $0.56\,\mathrm{c}$ and the LSB is preserved and the flow does not reattach. The large slot configuration triggers the transition where the air is injected and the flow reattaches and remains in a turbulent state.

$\zeta [x/c]$	clean airfoil	0.45		0.5		0.6	
L[x/c]	-	0.01	0.02	0.01	0.02	0.01	0.02
C_L	0.8241	0.591	0.433	0.599	0.217	0.432	0.27
C_D	0.01454	0.0285	0.0397	0.0277	0.0535	0.038	0.0459
C_L/C_D	56.7	20.7	10.9	21.6	4.05	11.3	5.9

Table 4 – Comparison of the aerodynamic performance of different configurations for an inclination of $\Psi=30^\circ$

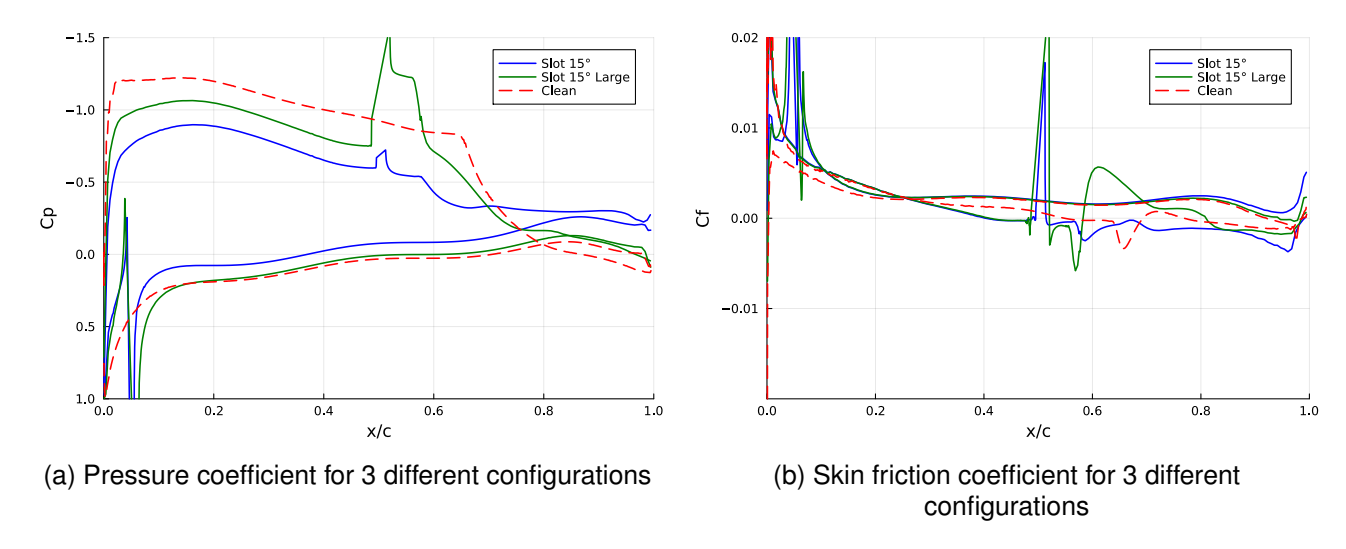


Figure 12 – Local physical quantities C_p and C_f obtained for $R_e = 5 \times 10^5$, $AoA = 5^{\circ}$, $\zeta = 0.5$, $\Psi = 15^{\circ}$

$\zeta [x/c]$	clean airfoil	0.45		0.5		0.6	
L[x/c]	-	0.01	0.02	0.01	0.02	0.01	0.02
C_L	0.8241	0.786	0.778	0.506	0.709	0.617	0.573
C_D	0.01454	0.0446	0.0429	0.039	0.0242	0.0332	0.0453
C_L/C_D	56.7	17.6	18.1	20.9	29.3	18.6	12.6

Table 5 – Comparison of the aerodynamic performance of different configurations for an inclination of $\Psi = 15^{\circ}$

7. Conclusions

The objective of this research was to investigate the performance of various PFC mechanisms on the DU89-134 airfoil using a combination of CFD simulations and experimental testing. Conducted at a specific operating point typical for HAPS, characterized by a Reynolds number of 500 000 and an angle of attack of 5°, the study focused on assessing the impact of a trip strip and a slot, with variations in location, inclination, and size, on aerodynamic efficiency.

The locations of separation and reattachment points for the trip strip configurations, obtained experimentally using Infrared Thermography (IRT), match the numerical predictions. This agreement validates the accuracy of the numerical setup.

The CFD results revealed that none of the configurations tested showed any improvement in aero-dynamic performance. Furthermore, experimental validation supported these findings. The comparison between RANS simulations and IR thermography indicated agreement when analyzing flow separation, transition, and reattachment. Although additional experiments such as Particle Image Velocimetry (PIV) or hot-wire anemometry could provide further insights into flow behavior, including velocity profiles and turbulent fluctuations, the collective results suggest that, at the specified design point, the implementation of PFCs did not yield any advantages; instead, they appeared to have a detrimental effect, possibly due to the low angle of attack chosen. It is important to note that this study only explored a limited set of PFCs under specific operating conditions, and the findings may not be universally applicable to all PFC types. Future research can focus on using high-fidelity numerical methods, such as URANS or LES, to solve unsteady flow. Future investigations could explore the effectiveness of VGs or cavities. Moreover, research at higher angles of attack, closer to stall conditions, could elucidate whether turbulent transition induced by these devices might delay stall.

8. Funding and Acknowledgements

This work was funded by the Belgian Royal Higher Institute for Defence for the project Numerics & Experiments on Low-Speed High-Altitude Wings (NELSHAW) under grant MSP21-02.

9. Contact Author Email Address

Contact the authors at: mail@carlobrunelli.com and matija.avirovic@mil.be

10. Copyright Statement

The authors confirm that they, and/or their company or organization, hold copyright on all of the original material included in this paper. The authors also confirm that they have obtained permission, from the copyright holder of any third-party material included in this paper, to publish it as part of their paper. The authors confirm that they give permission, or have obtained permission from the copyright holder of this paper, for the publication and distribution of this paper as part of the ICAS proceedings or as individual off-prints from the proceedings.

References

- [1] Adrián García-Gutiérrez, Jesús Gonzalo, Diego Domínguez, Deibi López, and Alberto Escapa. Aerodynamic optimization of propellers for high altitude pseudo-satellites. *Aerospace Science and Technology*, 96, 1 2020.
- [2] Amith Seshagiri, Evan Cooper, , and Lance W. Traub. Effects of vortex generators on an airfoil at low reynolds numbers. *Journal of Aircraft*, 46:116–122, 2009.
- [3] Emre Güler, Tahir Durhasan, İlyas Karasu, and Hurrem Akbiyik. Passive flow control around naca 0018 airfoil using riblet at low reynolds number. *Journal of the Institute of Science and Technology*, 11:2208–2217, 9 2021.
- [4] Jolan Wauters, Joris Degroote, and Jan Vierendeels. Comparative study of transition models for high-angle-of-attack behavior. *AIAA Journal*, 57:2356–2371, 2019.
- [5] Nikolaos Mourousias, Adrián García-Gutiérrez, Ahmed Malim, Diego Domínguez Fernández, Benoît G. Marinus, and Mark C. Runacres. Uncertainty quantification study of the aerodynamic performance of high-altitude propellers. *Aerospace Science and Technology*, 133, 2 2023.
- [6] Matija Avirovic, Carlo Brunelli, Benoit G. Marinus, Joris Degroote, and Jeroen Van Beeck. Numerical and experimental study of laminar-turbulent transition on a laminar airfoil at low reynolds number. American Institute of Aeronautics and Astronautics, 6 2023.
- [7] Siemens Digital Industries Software. Simcenter STAR-CCM+, version 2022.1, 2022.
- [8] ANSYS Inc. Fluent, 2024 R1 24.1.0, 2023.
- [9] Mark Drela. XFOIL, 6.99, 2013.
- [10] Mustafa Serdar Genç, Kemal Koca, Hacımurat Demir, and Halil Hakan Açıkel. *Traditional and New Types of Passive Flow Control Techniques to Pave the Way for High Maneuverability and Low Structural Weight for UAVs and MAVs*.
- [11] Jinjun Wang and Lihao Feng. *Flow Control Techniques and Applications*. Cambridge University Press, 2019.
- [12] Mehrdad Nafar Sefiddashti, Mahdi Nili-Ahmadabadi, and Behnam Saeedi Rizi. Experimental study of effects of circular-cross-section riblets on the aerodynamic performance of risø airfoil at transient flow regime. *Journal of Mechanical Science and Technology*, 32:709–716, 2 2018.
- [13] T. Rajesh Senthil Kumar, Mohini Priya Kolluri, V. R. Gopal Subramaniyan, and A. D. Sripathi. Passive flow control strategies for low reynolds number airfoils. volume 954. IOP Publishing Ltd, 10 2020.
- [14] Michael Breuer. Effect of inflow turbulence on an airfoil flow with laminar separation bubble: An les study. *Flow, Turbulence and Combustion*, 101:433–456, 9 2018.
- [15] Stephan Schmidt and Michael Breuer. Source term based synthetic turbulence inflow generator for eddyresolving predictions of an airfoil flow including a laminar separation bubble. *Computers and Fluids*, 146:1–22, 3 2017.
- [16] Arif M. Althaf, Yashwanth S. Bangaru, Richard Fawcett, Vishwanatha M. Guled, Tushar G. Maloo, Pablo N. Gorgojo, Carola R. Sala, Alberto S. Felix, Tom-Robin Teschner, Tamás I. Józsa, Aurelien Borgoltz, Nanyaporn Intaratep, William J. Devenport, and Máté Szoke. Numerical modeling and tunnel specific considerations for cfd model development of low-speed wind tunnels. American Institute of Aeronautics and Astronautics (AIAA), 6 2023.
- [17] Mark Drela. XFOIL: An Analysis and Design System for Low Reynolds Number Airfoils. In Thomas J. Mueller, editor, Low Reynolds Number Aerodynamics, Berlin, Heidelberg, 1989. Springer Berlin Heidelberg.
- [18] Snorri Gudmundsson. The Anatomy of the Airfoil, pages 235–297. Elsevier, 2014.
- [19] Jan Windte, Ulrich Scholz, and Rolf Radespiel. Validation of the rans-simulation of laminar separation bubbles on airfoils. *Aerospace Science and Technology*, 10:484–494, 9 2006.

Passive flow control devices on a low-Reynolds DU89-134 airfoil

- [20] Dallyn W. Wynnychuk and Serhiy Yarusevych. Characterization of laminar separation bubbles using infrared thermography. *AIAA Journal*, 58(7):2831–2843, 2020.
- [21] Riyadh Belamadi, Abdelouaheb Djemili, Adrian Ilinca, and Ramzi Mdouki. Aerodynamic performance analysis of slotted airfoils for application to wind turbine blades. *Journal of Wind Engineering and Industrial Aerodynamics*, 151:79–99, April 2016.
- [22] Mark S. Istvan and Serhiy Yarusevych. Effects of free-stream turbulence intensity on transition in a laminar separation bubble formed over an airfoil. *Experiments in Fluids*, 59:52, 3 2018.